In vivo high field magnetic resonance imaging and spectroscopy of adult zebrafish

Kabli, S.

1 General introduction

Biomedical research depends on the use of animal models to understand the pathogenesis of human disease at the cellular and molecular level and to provide systems for developing and testing new therapies. Mammalian models, such as the mouse, have been pre-eminent in modeling human diseases, primarily because of the striking homology between mammalian genomes and the many similarities in the biology of mice and human beings, spanning from anatomy to cell biology and physiology. Despite the pre-eminence of the mouse in modeling human disease, several aspects of murine biology have limited its routine use in large-scale genetic and therapeutic screening. For example, although forward-genetic screens (1-4) and randommutagenesis-based reverse genetics (5, 6) are feasible in the mouse and are currently underway, they cannot be applied routinely on the desired scale because they require considerable staff and infrastructure support. Hence, such approaches in mice are limited to a few large projects, often operating as screening consortia. In this context, the zebrafish (*Danio rerio*) has emerged recently as a versatile and genetically tractable alternative vertebrate model system. Sophisticated mutagenesis and screening strategies on a large scale, and with an economy that is not possible in other vertebrate systems, have generated zebrafish models of a wide variety of human diseases.

The zebrafish has also proven to be a useful and relevant model for studying vertebrate development and organogenesis (7, 8). It exhibits high fecundity,

about 200 eggs per week per female. Embryos develop rapidly in fresh water externally to the mother and are therefore easily manipulated *ex utero*, while progressing from fertilized eggs to free swimming larvae in 60 h. In addition, zebrafish embryos are transparent. Visualization of all stages of organ development is relatively easy in the first few days of life when the fish is only a few millimetres in length, and this can be combined with manipulation of gene expression at RNA and protein levels. Gene expression can be induced using microinjection of specific vectors at very early stages and is generally highly effective for at least the first 2 days of development (9). Because it can easily take up chemicals from water, zebrafish is also used as a pharmacological tool in drug discovery and ecotoxicity research (10-12). As it can live in as little as a few microlitres of fluid, only micrograms of compound per assay are needed for screening. This facilitates screening of compounds, enabling *in vivo* analysis of compound action at much earlier stages and higher throughput than hitherto possible. Clearly, the zebrafish model combines the relevance of a vertebrate with the scalability of an invertebrate and, in many studies, could provide an interesting intermediate vertebrate model to laboratory small mammals.

1.1 Zebrafish as a model for Cancer

In recent years, zebrafish received strong attention from cancer researchers, after it was discovered that zebrafish can develop almost any type of cancer (13). A critical asset of zebrafish as a cancer model is that many tumors histologically resemble human tumors (14). In addition, more general cancer characteristics such as genomic instability, invasiveness, transplantability, and the existence of cancer stem cells (15) apply to zebrafish tumors as well,

and many tumor suppressor genes and oncogenes have been conserved. Further, the development of fish lines harboring oncogenic transgenes and their amenability to genetic and pharmacological testing also made zebrafish a favorable model. Cancer progression in zebrafish recapitulates many aspects of human disease and opens the door for studies to identify genetic and chemical modifiers of cancer (14, 16-20). The development of xenograft models allow the propagation and visualization of human cancer cells engrafted in optically transparent zebrafish (21-25). Numerous mutant or tissue-specific transgenic cancer fish lines are available (14, 16-20). Zebrafish can also efficiently absorb anticancer agents directly from water which makes this organism appealing for screening these compounds (20, 26). Taken together, these studies validate zebrafish as a *bona fide* cancer model.

Advanced melanoma is a devastating and lethal cancer (27). Melanoma arises from melanocytes, which are the pigment producing cells of human skin. Melanocytes can proliferate and give rise to various types of benign nevi, which are commonly referred to as moles. Transformed melanocytes can yield melanomas that initially grow radially in the epidermis. This is followed by the transition to a vertical growth phase that involves invasion through the basement membrane into the underlying dermis, preceeding metastasis.

There are many areas of melanoma biology that are underexplored. For example, the steps by which a normal melanocyte becomes or generates a melanoma cell are largely unknown. How the disease subverts properties of normal melanocytes and their neural crest progenitors has been a topic of recent investigations, and this will be a fertile area of research in the future.

Lastly, while great progress has been made in identifying genetic defects that contribute to melanoma (28), there are clearly many more genes that remain to be tied to this disease. And significant challenges in the clinical management of this disease remain. These challenges are reflected in a very poor overall prognosis for patients with advanced melanoma, largely because there is no non-invasive early diagnosis and no effective therapy. (29). Translational research that uses fundamental knowledge of a disease to develop diagnostic and therapeutic strategies holds promise for improving melanoma treatment. The zebrafish melanoma model has unique attributes that may lead to important insights at the interface of melanocyte biology and clinical medicine.

1.2 Zebrafish as a model for studying brain disorders

Due to similar basic organization of brain components as that of human, zebrafish is increasingly used as a model for studying brain disorders (30-34). However, till now, modelling a brain disease in zebrafish requires optically transparent embryonic or larval, rather than adult, stages for optical detection that allows real-time imaging of developing pathologies. Experimentation with adult animals is not possible with optical methods, while diseases like neurodegeneration occur mainly at later stages in life. Considerable knowledge concerning the embryonic development of the central nervous system of the zebrafish has been collected in recent years. In contrast, there is an apparent lack of information on the organization of the adult zebrafish brain (35).

The zebrafish brain aminergic systems share many structural properties with the mammalian systems and practically all important physiological systems

in the brain involve the modulatory aminergic neurotransmitters. Many of these are also involved in human central nervous system diseases, including Parkinson's disease, schizophrenia, Alzheimer's disease, and depression. The noradrenergic, serotonergic, and histaminergic systems are highly similar (30-34). The dopaminergic systems also show similarities with the major difference being a lack of dopaminergic neurons in zebrafish mesencephalon. Development of automated quantitative behavioral analysis methods for zebrafish and imaging systems of complete brain neurotransmitter networks have enabled comprehensive studies on these systems in normal and pathological conditions at early developmental stages. Alterations of brain dopaminergic systems with neurotoxin such as MPTP, that in humans and rodents induces Parkinson's disease, induces both changes in the zebrafish dopaminergic system and quantifiable abnormalities in motor behavior (32). Chemically-induced brain histamine deficiency causes an identifiable alteration in histaminergic neurons and terminal networks, and a clear change in swimming behavior and long-term memory. Combining the imaging techniques and behavioral methods with zebrafish genetics is likely to help reveal how the modulatory transmitter systems interact to produce distinct behaviors, and how they are regulated in pathophysiological conditions and diseases. Several transgenic zebrafish models for neurodegeneration, such as Parkinson disease (30, 34), Huntington disease (36) and Alzheimer's disease (33) have been developed in recent years. However, imaging adult zebrafish brain *in vivo* was not feasible.

MRI is an imaging technique that can provide access to adult zebrafish brain anatomy with good resolution. It has been applied at embryonic stages, but not yet in adult fish. In addition, MRI in conjunction with MRS can be

invaluable for studying disease at molecular levels. In the following paragraph, a brief introduction of MRI and MRS and its relevance to zebrafish imaging and spectroscopy is presented.

1.3 MRI theoretical background

Magnetic resonance imaging (MRI) is a well-established non-invasive, diagnostic medical imaging technique based on the nuclear magnetic resonance (NMR) phenomenon (37). Every tissue in the body has a specific chemical makeup and thus the strength of the hydrogen NMR response differs from tissue to tissue. MRI allows the anatomy inside the body to be seen in either tomographic images taken along at any angle through the body, or three-dimensional volume images. The NMR information present in each pixel of one of these images is both temporal and spectral in nature. Conventional MRI relies on differences in a weighted average of the spectral and temporal information collected from different species to facilitate the diagnosis of diseases.

MR is based upon the interaction between an applied magnetic field and a nucleus with a nuclear magnetic moment or "spin" (37-39). Several nuclei, including ^{1}H, ^{31}P, ^{13}C, ^{15}N, and ^{19}F have nuclear magnetic moments corresponding with spin ½ and are most suitable for detection by magnetic resonance (38-40). Protons are the most abundant spin ½ nuclei in living organisms and they have the best NMR sensitivity (38-40). For this reason protons are the most frequently studied nuclei. As a crude simplification, nuclear spins can be thought of as small magnets. When placed in an external magnetic field (B_0) a large number of proton spins will be aligned parallel to B_0, with a somewhat smaller number oriented anti-parallel. This

orientation yields a net nuclear magnetization and a net magnetization vector M_z parallel to B_0.

After the RF pulse is switched off, the net magnetization vector will start reverting back to its equilibrium state as a result of a process which is called relaxation. The recovery process along the longitudinal axis is called T_1 relaxation, spin-lattice relaxation or longitudinal relaxation (Fig. 1A) and is described as:

$$M_z(t) = M_{z_{\max}}(1 - e^{-\frac{t}{T_1}}) \tag{1.1}$$

During a T_1 process, the nuclei are giving up energy to their immediate surroundings.

The dephasing process in the transverse plane (the plane orthogonal to B_0) is referred to as T_2 relaxation, or spin-spin relaxation.
In the T_2 process, nuclei exchange energy with each other and the spins lose phase coherence. Therefore to first order the net magnetization in the *xy*-plane decays exponentially to zero over time. The rate at which this occurs is dependent on T_2 (Fig. 1B) and the T_2 process is described as:

$$M_{xy}(t) = M_{xy_{\max}} e^{-\frac{t}{T_2}} \tag{1.2}$$

In reality the signal will decay at shorter relaxation time T_2 due to field inhomogeneities and magnetic susceptibility differences. This shorter relaxation time is known as T_2^*, and can be determined according to

$$\frac{1}{T_2^*} = \frac{1}{T_2} + \frac{1}{T_{2M}} + \frac{1}{T_{2MS}} \tag{1.3}$$

Here T_{2M} is the dephasing due to inhomogeneity of the applied field, and T_{2MS} is the dephasing due to magnetic susceptibility differences (40).
An RF coil placed perpendicular to the transverse plane will detect the transverse component of the net magnetization vector as it precesses around B_0. The length of the magnetization vector is the magnitude of the signal, while the angle between the magnetization vector and the y-axis is referred to as the the transverse plane after a single RF pulse is known as the free induction decay. Depending on the sample the FID can contain multiple resonance frequencies. A simple spectrum can be obtained from the FID by converting it from the time domain to the frequency domain using the Fourier transform. The resulting spectrum contains peaks for the various different frequencies contained within the FID.

To spatially resolve the NMR signal for MRI, an additional step is required. Spatial variations in frequencies can be translated to spatial information and subsequently to an image. Assigning spatial information to the spins is achieved by adding a magnetic field gradient inside the MR scanner. The gradient field in MRI is usually parallel to B_0. The gradient has three components, G_x, G_y, and G_z, associated with the x, y, or z spatial axis, respectively. The spins experience different field strengths depending on where they are within the gradient field. Positional dependence of the field strength and resonance frequencies can be calculated according to:

(A)

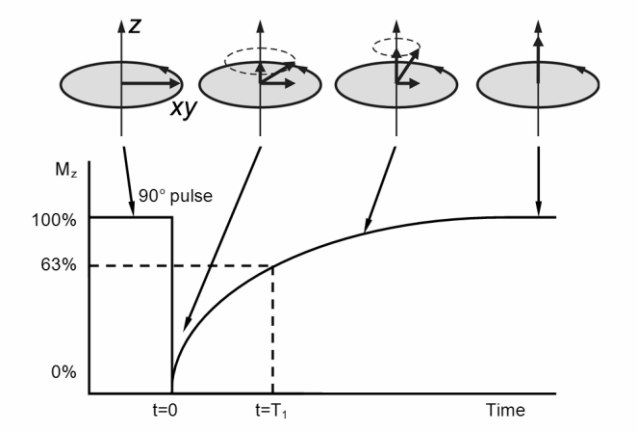

(B)

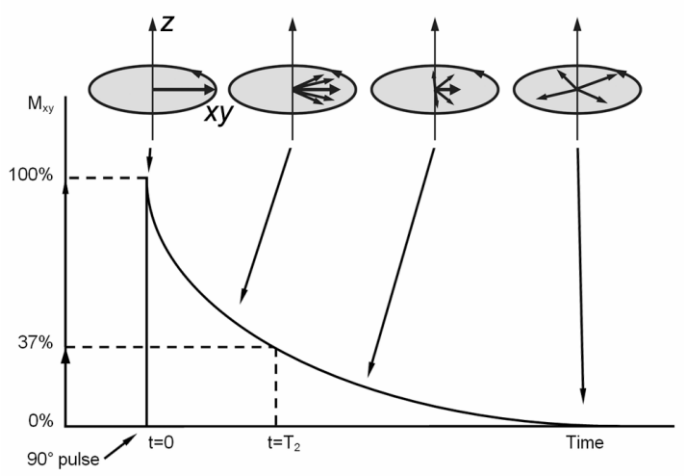

Figure 1.1 *(A): Re-growth of the longitudinal magnetization M_z and the definition of T_1; M_z will return to its original distribution along the z-axis through T_1 relaxation (eq. 1.1) . (B) Decay of the transverse magnetization M_{xy} and the definition of T_2; Loss of phase coherence, and thereby loss of magnetization in the xy-plane, is determined by T_2 relaxation (eq. 1.2).*

$$B(r) = B_0 + rG \tag{1.4}$$

$$\omega(r) = \gamma B(r) = \gamma B_0 + \gamma rG \tag{1.5}$$

Here $B(\mathbf{r})$ and $\omega(\mathbf{r})$ are the position dependent field strength and resonance frequency, respectively. The position in the magnetic field is denoted by the vector $\mathbf{r}$ and the magnitude and direction of the gradient is represented by $\boldsymbol{G}$ (1.4). Spins in different volume units within the field gradient experience a different magnetic field, and are associated with a different Larmor frequency. The selection of the desired cross-section or "slice" is achieved by applying a gradient along the *z*-axis in combination with an excitation pulse of a convenient bandwidth and shape (*e.g.* Sinc or hermite). This RF pulse excites only the spins in the desired slice, while leaving adjacent spins unaffected, as they have a different resonance frequency due to the applied *z*-gradient. Within the acquired slice, *x*- and *y*-gradients are applied to assign the spins at each position within the slice with a unique frequency and phase. The gradients in this example are often referred to as the slice selection- (G_z), the frequency encoding- (G_x) and the phase encoding gradients (G_y). G_x is usually kept constant over the course of an experiment, thus assigning a different frequency to each position along the *x*-axis. G_y is stepped a number of times each scan, depending on the desired resolution in the *y*-direction. G_y applies a specific phase angle to the transverse magnetization vector. While G_y is switched on, each transverse magnetization vector has its own unique Larmor frequency. When G_y is subsequently switched off, the spins return to the frequency they had prior to phase encoding, however, the phase angle of each transverse magnetization vector is different. A variety of imaging pulse sequences can

be created by combining slice selection, phase encoding and frequency encoding.

What distinguishes the T_2 process from its T_1 counterpart is that the magnitude of the field changes over the dephasing period is important, rather than the rate of their fluctuations. As far as biological tissue imaging is concerned, nature offers us a convenient handle in the form of T_1 and T_2 for constant discrimination. Generally, T_2 values are about one-tenth of the T_1 values for soft biological tissues, which have sufficiently different T_2 values to allow them to be differentiated by contrast on T_2-weighted images.

Among the most important and widely used pulse sequences for MRI are the spin echo sequence and the gradient echo sequence. Gradient Echo (GE) sequences use slice selective pulses of 90° or less, and subsequently employ the gradient coils for producing an echo (Fig. 1.2). This is done by first applying a negative frequency-encoding gradient, which is subsequently reversed, causing the spins to rephase and form an echo. Following signal detection the phase coherence of the precessing spins in the transverse plane is dephased or "spoiled" using spoiler gradients, thus ensuring contribution of only the longitudinal magnetization to the net magnetization **M** at the time of the next excitation pulse (40). Conversely, SE sequences use a slice selective 90° pulse for excitation, followed by a 180° pulse at t = TE/2. The 180° pulse serves to reverse or refocus the transverse magnetization. This produces an echo at t = TE. During SE acquisition, the phase encoding gradient is applied following the 90° pulse, and the frequency encoding, or read out-, gradient is applied centered around the echo at t = TE (40). The TE in these examples is the echo time, and is measured from the center of the excitation pulse to the center of the echo. As multiple excitation-refocus-

echo steps are needed to build up an entire image, the sequence is looped several times, depending on the desired resolution. The repetition time is defined as the time from the start of one loop of the sequence to the next.

1.3.1 Rapid acquisition with relaxation-enhancement imaging

Rapid acquisition with relaxation-enhancement imaging (41) is a fast spin echo imaging sequence in which multiple spin echoes are generated by employing multiple 180° refocusing pulses (Fig. 1.2). Each refocused echo is acquired after having experienced a different phase-encoding value.

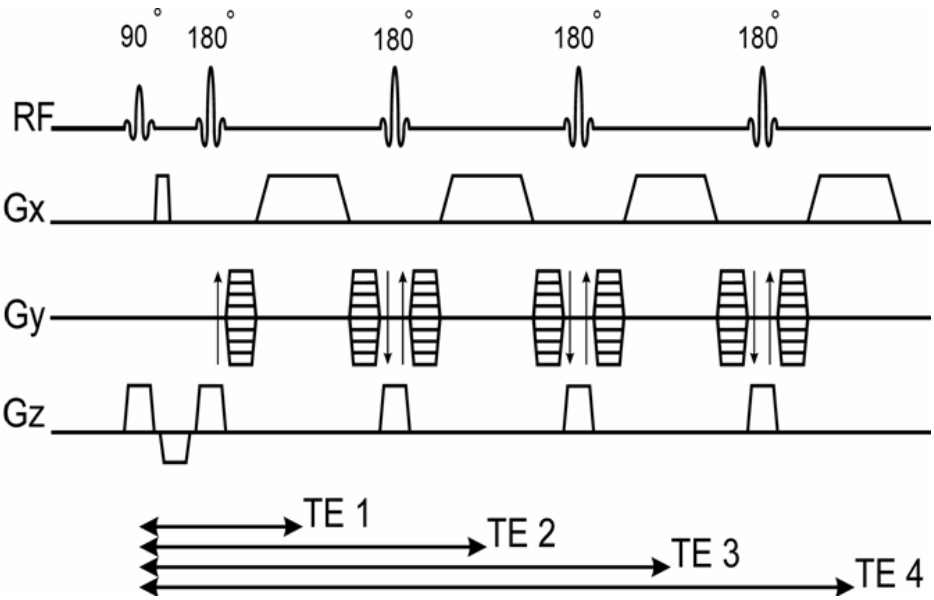

Figure 1.2: RARE pulse sequence: A four-segment (RARE factor of 4) version is shown. Each cycle has four phase encoding steps; the sequence will be looped until the desired number of phase encoding steps is reached. As this sequence acquires four times the data per loop as a standard SE sequence, the scan time is roughly 25% shorter than for an equivalent SE sequence. The effective TE is the TE time during which the $G_y = 0$ lines of data are acquired (4).

Because refocusing of the transverse magnetization is inherent in the sequence, it is less vulnerable to susceptibility-induced dephasing than gradient echo sequences, but it is substantially faster to apply than a spin-echo sequence with a single-phase encoding step per repetition time.

The primary contrast is T_2-based, although this can be mixed with T_1 and perfusion effects by combining it with the inversion recovery sequence (IR-RARE). The contrast in the final image can be modified depending on the choice of TE and TR. Choosing a long TR, and a relatively long TE, for example, will yield a T_2-weighted image, where elements with long T_2 will appear bright, and elements with a short T_2 will appear dark. A practical implementation of RARE imaging in visualizing *in vivo* zebrafish is demonstrated in chapter 2 and 4.

1.3.2 Transverse relaxation mapping

Intrinsic MR parameters, such as transverse (T_2) relaxation times are sensitive to changes in the biophysical environment of water, and are thought to be affected during impared cell physiology. Disease mechanisms influence the composition of tissue, and can have an effect on the tissue specific relaxation rates. Thus T_2 mapping can be used to diagnose or predict disease. For example, T_2 mapping can be used to delineate the disease volume. The regional distribution of T_2 values within a tumor is a measure of the tissue heterogeneity within the tumor volume (42). In addition, the large differences in T_2 relaxation times between normal and diseased tissue can be used in a computer algorithm to automatically demarcate the boundary of abnormal tissue.

Since the polarization present in the *xy*-plane depends on T_2, while different T_2-weighting factors are obtained by modifying the TE value of a spin echo technique, it is possible to calculate the value of T_2 from a series of SE images with different echo times. As the signal intensity in these images is related to the magnetization in the *xy* plane, T_2 can be calculated by substituting the measured signal intensity for $M_{xy}(t)$, according to

$$M_{xy}(t) = M_{xy_{\max}} e^{-\frac{t}{T_2}} \tag{1.6}$$

where *t* equals the experimental TE mentioned above.

This can be calculated for the individual voxels of the sample, thus creating a T_2 map, or for specific regions of interest, by averaging the signal intensities for the pixels located within the ROI, and calculating the average T_2 for that region. Since an SE technique is used here, the signal is rephased before detection, which causes the effects of field inhomogeneities and susceptibilities to cancel. Hence, the calculated T_2 is the "true" T_2 and not T_2^*. In chapter 4, T_2 mapping was used to monitor the heterogeneity of the tumors in zebrafish.

1.4 Magnetic Resonance Spectroscopy

In vivo magnetic resonance spectroscopy (MRS) is a unique method providing quantitative biochemical information from the selected volume of interest (VOI) inside the body non-invasively. It provides vital biological information at the molecular level. Combined with magnetic resonance imaging (MRI), an integrated MRI/MRS examination provides anatomical

structure, pathological function, and biochemical information about a living system. MRS provides a link between the biochemical alterations and the pathophysiology of disease. MRS has been widely applied in human and animal studies examining a variety of tissues (43-47).

The fundamental basis of MRS is governed by the same principles of nuclear magnetic resonance (NMR) (48, 49). MRS requires a magnetic field and a radio frequency (RF) transmit pulse at a particular resonant frequency to observe the signal of a specific nucleus (*e.g.*, ^{1}H, ^{31}P, ^{13}C etc.) in the region of interest. The product of MRS is a ‘‘spectrum’’ with a frequency axis in parts per million (ppm) and a signal amplitude axis (50-54). The signal amplitude measures a particular metabolite concentration. Specific nuclei (*e.g.*, ^{1}H) from the metabolite, depending on their characteristic signature, give rise to either a single peak or multiple peaks that are uniquely shifted along the frequency axis, depending on their chemical environment. The shift dispersion increases with magnetic field strength. *In vivo* ^{1}HMRS and ^{31}P-MRS are the most widely used applications of MRS, but other nuclei that are used for MRS studies include ^{13}C, ^{15}N, ^{19}F, and ^{23}Na.

A wide variety of spatial localization techniques are in use to localize the spectroscopic measurement in a specific volume of interest, or voxel. These methods rely on the spatial selection of slices by the application of frequency-selective RF pulses in the presence of a magnetic field gradient. Some of them require several acquisitions to achieve complete localization, whereas others can achieve localization in a single experiment (39). Among the most popular methods is point resolved spectroscopy (55, 56). The PRESS sequence is a double spin-echo sequence. Three slice-selective

pulses (90°, 180°, 180°) along three orthogonal axes define three orthogonal slices, and make it possible to localize the signal in the voxel formed by the intersection of the three slices. Outer volume suppression schemes excite narrow slices positioned around the volume of interest to selectively remove unwanted signals from outside the voxel. Following slice selective excitation, the transverse magnetization in these slices is dephased by a subsequent magnetic field crusher gradient. OVS is most commonly employed to remove lipid signals from the spectrum (39). As water is the most abundant compound in tissue, the NMR proton spectrum of almost all tissue is dominated by a resonance at ~4.7 ppm that originates from water protons. While metabolite detection is possible without water suppression, the water peak does lead to baseline distortions and spurious signals due to vibration-induced signal modulation, which makes the detection of metabolites unreliable (39). Suppression of the water signal eliminates these problems, leading to a reliable and consistent detection of metabolite spectra. Water signals can be eliminated by utilizing differences in relaxation parameters. One such method, VAPOR, combines T_1-based water suppression and optimized frequency-selective perturbations to provide excellent water suppression with a large insensitivity towards T_1 and B_1 inhomogeneity (39, 57). The combination of OVS and water suppression improves localization performance and reduces the demand for spoiler gradients (57). The PRESS sequence in combination with water and outer volume suppression schemes has been optimized for zebrafish brain in chapter 3.

MRS techniques have been developed and applied extensively in brain research (58). The brain has multiple levels of compartmentation ranging from the type of cellular compartment (neuron versus astrocyte) to the type

of tissue compartment (the gray matter vs. the white matter). These compartments are highly integrated and work together to attain various brain functions. MRS is useful in understanding the neurochemical changes in the brain due to different physiological processes. Many MRS applications have been reported exclusively in the brain due to the lack of motion artifacts in the brain. In addition, the brain is more or less spherical; hence, it is easier to adjust to a high degree of homogeneity of the magnetic field by shimming for MRS studies. However, there are susceptibility differences in the brain between the intracellular and extracellular space. The problems with sensitivity and susceptibility differences can become more serious when considering small zebrafish brain.

1.5 MRI/MRS at ultra-high magnetic field

Magnetic field strengths for *in vivo* MRI and MRS have seen a steady increase, and are currently up to 9.4 T for humans and 17.6 T for animals. This drive has largely been fueled by the greatly improved contrast-to-noise (CNR) ratio of functional MRI (fMRI) techniques, as well as the linear increase in signal-to-noise (SNR) ratio and spectral resolution with increasing field strength (59).

Since T_1 and T_2 relaxation parameters play an important role in the actual SNR and resolution, they should be critically considered while imaging at high-magnetic field. In general, T_1 relaxation times increase with increasing field strength, while the absolute differences between tissue T_1's become somewhat smaller. Therefore, overall the T_1 contrast will decrease at higher magnetic fields. However, since the SNR is improved at higher magnetic fields, the CNR is typically higher. It has been demosnstrated in earlier

studies that even at 9.4 T and 11.7 T high-quality T_1-weighted images can be obtained from rat brain (59), in close analogy to high-quality T_1-weighted human brain images reported at 7 T (60). Thus T_1-weighting remains a valuable image contrast mechanism even at very high magnetic fields. Water T_2 relaxation times decrease dramatically in high magnetic field. The relative differences in tissue T_2's remain the same or actually increase with increasing field strength. Therefore, while it may be more difficult to attain the shorter TE's required, T_2 weighting is a viable high-field image contrast mechanism, as shown by the excellent T_2 contrast obtained at 9.4 T in previous studies (61). For NMR spectroscopy a higher magnetic field strength is always desirable. The spectral resolution and the quantification accuracy of metabolites, especially those with strongly coupled spins and those present in low concentration, will continue to improve in moving toward increasingly high magnetic fields. Therefore, both the information content and the quantification accuracy of metabolites will improve at higher magnetic fields.

Thus, the use of high magnetic fields will be highly beneficial for MR imaging as well as MR spectroscopy of zebrafish. This can be achieved by using high (9.4T) and ultra-high magnetic fields (17.6T) in combination with strong magnetic field gradients and the use of small, high-sensitivity RF coils to achieve the necessary sensitivity.

1.6 Scope of the thesis

The necessity to study an adult zebrafish non-invasively and the recent developments in the field of MR microimaging and spectroscopy has brought us to use MR microimaging and spectroscopy as analysis tools to

visualize anatomical and molecular details of live adult zebrafish. Although a large pool of genome wide studies in zebrafish at early embryonic stages is available, *in vivo* studies in adult zebrafish are missing. Non-invasive studies of adult zebrafish performed in this thesis provide a means to bridge the gap between genetic studies at early embryonic stages and the structural and functional investigations at the adult stages. The specific aim of this thesis is to implement and optimize high resolution MR microimaging methods to obtain *in vivo* anatomical information from adult zebrafish. These methods were then successfully applied to investigate the presence of internal tumors in transgenic zebrafish. In addition, *in vivo* MR spectroscopy has been applied to detect metabolites in adult zebrafish brain for the first time.

In **chapter 2**, high-field μMRI methods have been optimized and successfully implemented to visualize anatomical details of adult zebrafish *in vivo*. Described in **chapter 3** is the implementation and optimization of a localized 1D MR spectroscopic sequence, at 9.4T. Using this sequence, highly resolved 1D MR spectra were obtained, for the first time, from the adult zebrafish brain *in vivo*. In **chapter 4**, μMRI was applied to track spontaneous melanomas in stable transgenic zebrafish model expressing a RAS oncoprotein and lacking P53. The heterogeneity of the tumor has been probed by measuring T_2 relaxation times in different regions of the tumors. **Chapter 5** provides a general discussion to the work presented in this thesis, and presents some future prospects.

References

1. Nolan PM, Peters J, Strivens M, Rogers D, Hagan J, Spurr N, Gray NC, Vizor L, Brooker D, Whitehill E, Washbourne R, Hough T, Greenaway S, Hewitt M, Liu X, McCormack S, Pickford K, Selley R, Wells R, Tymowska-Lalanne Z, Roby P, Glenister P, Thornton C, Thaung C, Stevenson JA, Arkell R, Mburu P, Hardisty R, Kiernan A, Erven A, Steel KP, Voegeling S, Guenet JL, Nickols C, Sadri S, Naase M, Isaacs A, Davies K, Browne M, Fisher EMC, Martin J, Rastan S, Brown SDM, Hunter J. A systematic, genome-wide, phenotype-driven mutagenesis programme for gene function studies in the mouse. Nature Genet 2000; 25:440–443.
2. Hrabe de Angelis MH, Flaswinkel H, Fuchs H, Rathkolb B, Soewarto D, Marschall S, Heffner S, Pargent W, Wuensch K, Jung M, Reis A, Richter T, Alessandrini F, Jakob T, Fuchs E, Kolb H, Kremmer E, Schaeble K, Rollinski B, Roscher A, Peters C, Meitinger T, Strom T, Steckler T, Holsboer F, Klopstock T, Gekeler F, Schindewolf C, Jung T, Avraham K, Behrendt H, Ring J, Zimmer A, Schughart K, Pfeffer K, Wolf E, Balling R. Genome-wide, large-scale production of mutant mice by ENU mutagenesis. Nature Genet 2000; 25:444–447.
3. Michaud EJ, Culiat CT, Klebig ML, Barker PE, Cain KT, Carpenter DJ, Easter LL, Foster CM, Gardner A, Guo ZY, Houser KJ, Hughes LA, Kerley MK, Liu Z, Olszewski RE,Pinn I, Shaw GD, Shinpock SG, Whyemore A, EM Rinchilk, Johnson DK. Efficient gene-driven germ-line point mutagenesis of C57BL/6J mice. BMC Genomics 2005; 6:164.
4. Carpinelli MR, Hilton DJ, Metcalf D, Antonchuk JL, Hyland CD, Mifsud SL, Rago LD, Hilton AA, Willson TA, Roberts AW, Ramsay RG, Nicola NA, Alexander WS. Suppressor screen in Mpl–/– mice: *c-Myb* mutation causes supraphysiological production of platelets in the absence of thrombopoietin signaling. Proc Natl Acad Sci USA 2004; 101:6553–6558.

5. Coghill EL, Higill A, Parkinson N, Davison C, Glenister P, Clements S, Hunter J, Cox RD, Brown SDM. A gene-driven approach to the identification of ENU mutants in the mouse. Nature Genet 2002; 30:255–256.
6. Quwailid MM, Hugill A, Dear N, Vizor L, Wells S, Horner E, Fuller Shelly, Weedon J, McMath H, Woodman P, Edwards D, Campbell D, Rodger S, Carey J, Roberts A, Glenister P, Lalanne Z, Parkinson N, Coghill EL, Mckeone R, Cox S, Willan J, Greenfield A, Keays D, Brady S, Spurr N, Gray I, Hunter J, Brown SDM, Cox RD. A gene-driven ENU based approach to generating an allelic series in any gene. Mamm Genome 2004; 15: 585–591.
7. Van der Sar AM, Appelmelk BJ, Vandenbroucke-Grauls CM, Bitter W. A star with stripes: zebrafish as an infection model. Trends Microbiol 2004;12:451–457.
8. Langenau DM, Zon LI. The zebrafish: a new model of t-cell and thymic development. Nat Rev Immunol 2005;5:307–317.
9. Westerfield M. The Zebrafish book. A guide for the laboratory use of Zebrafish (Danio rerio). University of Oregon Press:Eugene, OR, 1995.
10. Zon LI, Peterson RT. *In vivo* drug discovery in the zebrafish. Nat.Rev. Drug Discov. 2005; 4(1): 35–44.
11. Goldsmith P. Zebrafish as a pharmacological tool: the how, why and when. Current Opinion in Pharmacology 2004; 4(5): 504–512.
12. Ankley GT, Johnson RD. Small fish models for identifying and assessing the effects of endocrine-disrupting chemicals. ILAR J. 2004; 45(4): 469–483.
13. Kent ML, Spitsbergen JM, Matthews JM, Fournie JW, Westerfield M. Diseases of zebrafish in research facilities. Zebrafish International Resource Center 2002. Available from: http://zebrafish.org/zirc/health/diseaseManual.php.
14. Amatruda JF, Shepard JL, Stern HM, Zon LI. Zebrafish as a cancer model system. Cancer Cell 2002; 1:229-231.

15. Langenau DM, Keefe MD, Storer NY, Guyon JR, Kutok JL, Le X, Goessling W, Neuberg DS, Kunkel LM, Zon LI. Effects of RAS on the genesis of embryonal rhabdomyosarcoma. Genes Dev 2007;21:1382 – 1395.
16. Smolowitz R, Hanley J, Richmond H. A three-year retrospective study of abdominal tumors in zebrafish maintained in an aquatic laboratory animal facility. Biol Bull 2002;203:265 –266.
17. Stern HM, Zon LI. Cancer genetics and drug discovery in the zebrafish**.** Nature Revieuws Cancer 2003;3:1-7.
18. Berghmans S, Murphey RD, Wienholds E, Neuberg D, Kutok JL, Fletcher CDM, Morris JP, Liu TX, Schulte-Merker S, Kanki JP, Plasterk R, Zon LI, Look AT. tp53 mutant zebrafish develop malignant peripheral nerve sheath tumors. Proc Natl Acad Sci U S A 2005;102:407 – 412.
19. Goessling W, North TE, Zon LI. Ultrasound biomicroscopy permits *in vivo* characterization of zebrafish liver tumors. Nat Methods 2007; 4:551-553.
20. Kari G, Rodeck U, Dicker AP. Zebrafish: an emerging model system for human disease and drug discovery. Clin Pharmacol Ther 2007; 82: 70–80.
21. Haldi M, Ton C, Seng WL, McGrath P. Human melanoma cells transplanted into zebrafish proliferate, migrate, produce melanin, form masses and stimulate angiogenesis in zebrafish. Angiogenesis . 2005; 9: 139–151.
22. Lee LM, Seftor EA, Bonde G, Cornell RA, Hendrix MJ. The fate of human malignant melanoma cells transplanted into zebrafish embryos: assessment of migration and cell division in the absence of tumor formation. Dev Dyn 2005; 233: 1560–1570.
23. Topczewska JM, Postovit LM, Margaryan NV, Sam A, Hess AR, Wheaton WW, Nickoloff BJ, Topszewski J, Hendrix MJC. Embryonic and tumorigenic pathways converge via Nodal signaling: role in melanoma aggressiveness. Nat Med 2006;12: 925–932.
24. Nicoli S, Ribatti D, Cotelli F, Presta M. Mammalian tumor xenografts induce neovascularization in zebrafish embryos. Cancer Res 2007; 67: 2927–2931.

25. Stoletov K, Montel V, Lester RD, Gonias SL, Klemke R. High-resolution imaging of the dynamic tumor cell vascular interface in transparent zebrafish. Proc Natl Acad Sci USA 2007;104:17406–17411.
26. Parng C, Seng WL, Semino C, McGrath P. Zebrafish: a preclinical model for drug screening. Assay Drug Dev Technol 2002;1: 41–48.
27. Ceol CJ, Houvras Y, White RM, Zon LI. Melanoma biology and the promise of zebrafish. Zebrafish 2008; 4:247-255.
28. Chin L, Garraway LA, Fisher DE. Malignant melanoma: genetics and therapeutics in the genomic era. Genes Dev 2006; 20:2149–2182.
29. Lorigan P, Eisen T, Hauschild A. Systemic therapy for metastatic malignant melanoma—from deeply disappointing to bright future? Exp Dermatol 2008;17:383–394.
30. Bretaud S, Allen C, Ingham PW, Bandmann O. p53-dependent neuronal cell death in a DJ-1-deficit zebrafish model of Parkinson's disease. J Neurochem 2007; 100:1626–1635.
31. Tomasiewics HG, Flaherty DB, Soria JP, Wood JG. Transgenic zebrafish model of neurodegeneration. J Neurosci Res 2002;70:734-745.
32. Panula P, Sallinen V, Sundvik M. Modulatory neurotransmitter systems and behavior: towards zebrafish models of neurodegenerative diseases. Zebrafish 2006;3:235-247.
33. Campbell WA, Yang H, Zetterberg H. Zebrafish lacking Alzheimer presenilin enhancer 2 (Pen-2) demonstrate excessive p53-dependent apoptosis and neuronal loss. J Neurochem 2006; 96:1423-1440.
34. Bai Q, Mullett SJ, Garver JA, Hinkle DA, Burton EA. Zebrafish DJ-1 is evolutionarily conserved and expressed in dopaminergic neurons. Brain Res 2006; 1113:33-44.
35. Rupp B, Wullimann MF, Reichert H. The zebrafish brain: a neuroanatomical comparison with the goldfish. Anat Embryol 1996;194: 187–203.

36. Flinn L, Bretaud S, LO C, Ingham PW, Bandmann O. Zebrafish as a new animal model for movement disorders. Journal of Neurochemistry 2008; 106: 1991-1997.
37. Levitt MH. Spin dynamics: basics of nuclear magnetic resonance, 1st ed. Wiley 2001, Chichester, UK.
38. Haacke EM, Brown RW, Thompson MR, Venkatesan R. Magnetic resonance imaging: physical principles and sequence design, 1st ed. Wiley-Liss 1999, Hoboken, USA.
39. De Graaf RA. *In vivo* NMR spectroscopy: principles and techniques, 2nd ed. Wiley 2008; Chichester, UK.
40. Brown MA, Semelka RC. MRI: basic principles and applications, 3rd ed. Wiley-Liss 2003, Hoboken, USA.
41. Hennig J, Nauerth A, Friedburg H. Rare imaging - a fast imaging method for clinical MR. Magn Reson Med 1986;3:823-833.
42. Bloch P, Lenkinski RE, Buhle, Jr. EL, Hendrix R, Bryer M, McKenna WG. The use of T_2 distribution to study tumor extent and heterogeneity in head and neck cancer. Magn Reson Imaging 1991; 9:205-211.
43. Boesch C. Musculoskeletal spectroscopy. J Magn Reson Imaging 2007;25(2):321-338.
44. Cecil KM. MR spectroscopy of metabolic disorders. Neuroimaging clinics of North America 2006;16(1):87-116.
45. Choi JK, Dedeoglu A, Jenkins BG. Application of MRS to mouse models of neurodegenerative illness. NMR in biomedicine 2007; 20(3):216-237.
46. Rosen Y, Lenkinski RE. Recent advances in magnetic resonance neurospectroscopy. Neurotherapeutics 2007;4(3):330-345.
47. Sibtain NA, Howe FA, Saunders DE. The clinical value of proton magnetic resonance spectroscopy in adult brain tumours. Clinical radiology 2007;62(2):109-119.
48. Ernst R. Nuclear magnetic double resonance with an incoherent radio-frequency field. J Chem Phys 1966; 45:3845–3861.

49. Mandal PK, Majumdar A. A comprehensive discussion of HSQC and HMQC pulse sequences. Concepts Magn Reson 2004; Part A 20A:1–23.
50. Pettegrew JW, Panchalingam K, Moossy J, Martinez J, Rao G. Correlation of phosphorus-31magnetic resonance spectroscopy and morphologic findings in alzheimer's disease. Arch Neurol 1988; 45: 1093–1096.
51. Moonen CT, von Kienlin M, van Zijl PC, Cohen J, Gillen J. Comparison of single-shot localization methods (STEAM and PRESS) for *in vivo* proton NMR spectroscopy. NMR Biomed 1989; 2:201–208.
52. Van der Toorn A, Dijkhuizen RM, Tulleken CA, Nicolay K. T_1 and T_2 relaxation times of the major ^{1}H-containing metabolites in rat brain after focal ischemia. NMR Biomed 1995;8:245–252.
53. Stanley JA. *In vivo* magnetic resonance spectroscopy and its application to neuropsychiatric disorders. Can J Psychiatry 2002;47:315–326.
54. Moonen CTW, Sobering G, Vanzijl PCM, Gillen J, Vonkienlin M, Bizzi A. Proton spectroscopic imaging of human brain. J Magn Reson 1992; 98:556–575.
55. Bottomley PA. Selective volume method for performing localized NMR spectroscopy. US patent 1984;4:480-228.
56. Bottomley PA. Spatial localization in NMR spectroscopy *in vivo*. Ann N Y Acad Sci 1987; 508:333-348.
57. Tkac I, Starcuk Z, Choi IY, Gruetter R. *In vivo* H-1 NMR spectroscopy of rat brain at 1 ms echo time. Magn Reson Med 1999;41:649-656.
58. Gillies RJ, Morse DL. *In vivo* magnetic resonance spectroscopy in cancer. Annu Rev Biomed Eng 2005; 7:287–326.
59. De Graaf RA, Brown PB, McIntyre S, Nixon TW, Behar KL, Rothman DL. High magnetic field water and metabolite proton T_1 and T_2 relaxation in rat brain *in vivo*. Magnetic Resonance in Medicine 2006; 56:386–394.
60. Henry PG, Kim SG, Lieu H, Tkac I, Vaughan T, Van De Moortele PF, Yacoub E, Zhu XH. Ultrahigh field magnetic resonance imaging and spectroscopy. Magn Reson Imaging 2003;21:1263–1281.

61. Braakman N, Matysik J, van Duinen SG, Verbeek F, Schliebs R, de Groot HJM, Alia A. Longitudinal assessment of alzheimer's β-Amyloid plaque development in transgenic mice monitored by *in vivo* magnetic resonance microimaging. J Magn Res Imaging 2006;24:530-536.